# SlowPoke: Understanding and Detecting On-Chip Fail-Slow Failures in Many-Core Systems

Junchi Wu Peking University Beijing, China 2501111908@stu.pku.edu.cn

Yuyang Jin Tsinghua University Beijing, China jyy17@mails.tsinghua.edu.cn Xinfei Wan Peking University Beijing, China 2300013096@stu.pku.edu.cn

> Guangyu Sun Peking University Beijing, China gsun@pku.edu.cn

Zhuoran Li Peking University Beijing, China 2200012710@stu.pku.edu.cn

> Yun Liang Peking University Beijing, China ericlyun@pku.edu.cn

Diyu Zhou Peking University Beijing, China diyu.zhou@pku.edu.cn

#### Abstract

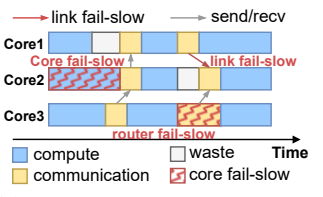
Many-core architectures are essential for high-performance computing, but their performance is undermined by wide-spread fail-slow failures. Detecting such failures on-chip is challenging, as prior methods from distributed systems are unsuitable due to strict memory limits and their inability to track failures across the hardware topology.

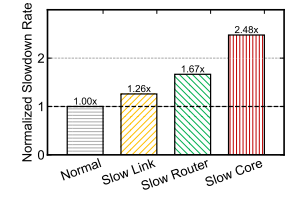
This paper introduces SlowPoke, a lightweight, hardware-aware framework for practical on-chip fail-slow detection. SlowPoke combines compiler-based instrumentation for low-overhead monitoring, on-the-fly trace compression to operate within kilobytes of memory, and a novel topology-aware ranking algorithm to pinpoint a failure's root cause. We evaluate SlowPoke on a wide range of representative many-core workloads, and the results demonstrate that SlowPoke reduces the storage overhead of detection traces by an average of 115.9×, while achieving an average fail-slow detection accuracy of 86.77% and a false positive rate (FPR) of 12.11%. More importantly, SlowPoke scales effectively across different many-core architectures, making it practical for large-scale deployments.

# 1 Introduction

Many-core architectures, which integrate tens to thousands of processing cores on a single chip or via multi-chiplet integration, are becoming central to modern high-performance computing. Characterized by their massive parallelism and high aggregate throughput, these processors are designed to accelerate today's most demanding workloads, including deep neural networks [13, 14, 72, 74, 80], large-scale graph analytics [11, 16, 57], and scientific simulations [2, 46, 62]. As a result, many-core architectures are increasingly popular from edge platforms to supercomputers, often delivering

Youwei Zhuo Peking University Beijing, China youwei@pku.edu.cn





- **(a)** Fail-slow failures on different hardware components.
- **(b)** Normalized execution time of ResNet-50.

**Figure 1.** Fail-slow failure and its impact on overall performance. Execution times are measured on a  $4\times4$  core processor with a  $10\times$  performance degradation fail-slow of different components.

significant gains in performance and energy efficiency compared to traditional multi-core CPUs [34, 41, 66, 67].

However, the scale and complexity of many cores introduce a critical reliability challenge: the fail-slow failure [22]. Unlike failures that result in system crashes [3, 51] or incorrect outputs [10], a fail-slow failure allows a hardware component to remain functionally correct but operate at a significantly reduced speed. The causes are both complex and widespread, spanning multiple layers of the system. First, at the device level, physical degradation from effects like aginginduced transistor and interconnect wear can cause timing violations that reduce operational frequency [1, 5, 23, 65]. Concurrently, thermal stress introduce dynamic system-wide slowdowns [83]. For example, under heavy workloads, extreme temperatures in DRAM can trigger protective states that cut performance by 24% to 52% [40, 50, 55]. Finally, bottlenecks emerge from shared resource contention and software bugs as cores compete for access to caches, memory, or the on-chip network [6, 71].

The performance impact of these failures is especially severe in parallel applications where tasks are interdependent.

1

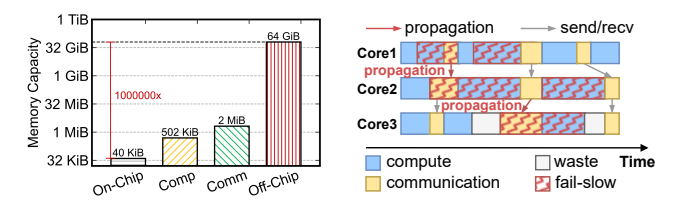


**Figure 2.** Challenges for detecting fail-slow failures in many-core processors: (a) On-chip, off-chip memory capacity versus computation and communication tracing log size for tracing DarkNet-19 for 1 second on a 4×4 core processor. (b) Slowdown propagates across cores along communication dependencies.

In these workloads, progress is often dictated by the slowest-performing task—a phenomenon known as the straggler effect. A single slow core or link can stall numerous otherwise healthy components, leaving expensive parallel hardware idle [39, 42, 43, 70]. Our simulations quantify this cascading impact: as shown in Figure 1b, a single fail-slow event in a link, router, or core increases total execution time by 1.26×, 1.67×, and 2.48×, respectively. This demonstrates that fail-slow behavior can negate the benefits of massive parallelism, posing a critical barrier to building efficient and scalable many-core systems.

Several approaches exist for detecting fail-slow failures in large-scale parallel and distributed systems. One common strategy is runtime tracing, which collects detailed event logs during execution [33, 77]. Another is graph-based analysis, which constructs a dependency graph of the software tasks. By analyzing communication patterns and critical paths within this graph, these methods identify applicationlevel stragglers that are holding up the overall computation [20, 32, 64]. However, these strategies are not a good fit for on-chip detection due to two major challenges. First, runtime tracing is constrained by strict on-chip memory limits. For example, it takes 502 KiB and 2 MiB of storage to trace the communication and computation of a 16-core processor for just one second (Figure 2), while a single core has typically less than 64 KiB of available SRAM. This makes logging impractical and and forces a difficult trade-off between monitoring overhead and accuracy. Second, graphbased analysis struggles with **on-chip failure propagation**. A slowdown in one hardware component quickly spreads to its neighbors, hiding the true source. Because existing graph-based methods analyze the software tasks and ignore the underlying hardware topology, they often misidentify the source, blaming a component that is merely slowed by a bottleneck elsewhere on the chip.

Therefore, an effective detection mechanism for many-core systems must be both **lightweight** to be efficient and **hardware-aware** to be accurate. A lightweight design must compress data on-the-fly and operate within tight memory limits, while a hardware-aware approach must analyze the

chip's hardware topology to trace a slowdown back to its true origin.

In this paper, we present **SlowPoke**<sup>1</sup>, a fail-slow detection framework with a comprehensive workflow that spans data collection, storage, and analysis to meet these requirements. First, we propose an eBPF-like probe mechanism that enables lightweight and accurate performance data tracing without interfering with program execution. The probes are defined by a configurable tuple, allowing users to precisely specify insertion points. We further design a sketch-based data structure to compress and store the collected traces efficiently. To narrow down the failure candidates, we employ a groupbased fail-core detection in combination with underdetermined linear system-based fail-link inference. To capture both software and hardware propagation of fail-slow failures, we reconstruct the communication dependency graph onto the hardware topology, and incorporate temporal information through hierarchical graph. Finally, we introduce FailRank, an iterative ranking algorithm that computes a fail-slow score for each component, thereby identifying the most likely root cause of fail-slow failures. In summary, our contributions are:

- SL-Compiler: A programmable fail-slow probe mechanism that leverages compiler-based instrumentation.
   This allows for fine-grained, customizable event monitoring at runtime with minimal execution overhead.
- SL-Recorder: A compact, on-the-fly, sketch-based data structure that filters and compresses trace data. This design preserves critical failure signatures while operating within the strict memory constraints of onchip SRAM.
- **SL-Tracer**: A topology-aware, multi-stage diagnosis pipeline that integrates the software communication graph with the hardware topology. It uses a novel algorithm—FailRank—to accurately trace failure propagation across cores and links, and pinpoint the true root cause.

We evaluate SlowPoke on a many-core simulation platform using representative many-core worloads and injected fail-slow failures. Experimental results show that, on average, SlowPoke reduces the storage overhead of detection traces by 115.9×, achieves 86.77% fail-slow detection accuracy with 12.11% FPR, and scales effectively to larger core counts.

# 2 Background

#### 2.1 Many-Core Architectures

Many-core architectures integrate cores into a scalable onchip network to exploit massive parallelism. Figure 3 illustrates the fundamental components of such an architecture. Inter-core communication is enabled by the on-chip network, which can adopt a variety of topologies. Common structures

<sup>&</sup>lt;sup>1</sup>The source code of \$1owPoke along with failure datasets and traces are available at https://github.com/pku-lemonade/sloth

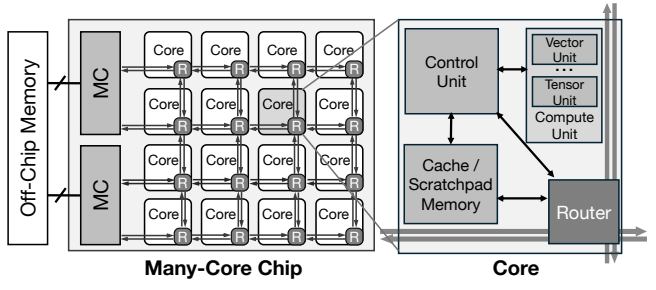


**Figure 3.** Overview of a many-core architecture with 2D-mesh network and its intra-tile organization.

include 2D-mesh, torus, and ring networks [17, 80], while more complex topologies such as hypercube and dragonfly have also been proposed [18]. These topologies can support different communication patterns and, in specific scenarios, provide higher bandwidth. In this work, we focus on meshbased networks, as they are implementation-friendly and are the most widely adopted topology in practice [21, 61]. Each core is directly connected to a router and consists of three major components: a control unit, a compute unit, and a scratchpad memory. The control unit manages intra-core resource allocation and task scheduling. The compute unit executes application workloads and integrates heterogeneous accelerators such as vector units or tensor units, depending on requirements. The scratchpad memory is a small, highspeed SRAM placed adjacent to the compute unit, typically less than 64 KiB in capacity. It is explicitly managed by software or compilers, thereby simplifying hardware coherence logic [4, 15].

Based on the hardware organization above, many-core systems often employ a dataflow execution model to maximize concurrency and overlap computation with communication [7, 9, 27]. In this paradigm, programs are represented as computation graphs, where nodes denote operations and edges represent data dependencies[12, 48]. Execution is data-driven—an operation is triggered as soon as its input data becomes available, avoiding the cost of global synchronization. Tasks are mapped onto cores according to data locality and computational workflow, while the scheduler within each core monitors operation readiness, fetches operands from local or neighboring cores, and dispatches them to compute units. Intermediate results are routed through the NoC according to the communication pattern derived from the computation graph. This fine-grained pipelining of data movement and processing improves utilization, but also creates tight coupling between cores: delays in one core's execution can propagate through dependent operations across the chip, amplifying the performance impact of fail-slow failures.

# 2.2 Hardware Failures

In many-core systems, hardware components are subject to a wide range of failures, which may manifest in different ways but invariably influence normal program execution. Based on this behavior, common hardware failures can be broadly classified into two categories: fail-slow and fail-stop[22, 49].

For cores, bit flips can alter register values, leading to incorrect computation results or even program crashes [26, 54], which are characteristic of fail-stop failures. In contrast, performance variations caused by internal resource contention, workload imbalance, or hardware aging typically degrade overall performance [60, 82], and are categorized as fail-slow failures. For memory, permanent physical defects as well as software bugs or mismanagement can trigger system crashes, thus are fail-stop failures. Meanwhile, memory leaks or buffer overflows could consume significant system resources, causing response delays and performance degradation, which belong to fail-slow failures [43, 73]. For NoC, transient bandwidth reductions on links or low router port utilization can decrease overall throughput and prolong program execution time[8, 63], both of which are fail-slow failures. In contrast, routing-induced deadlocks can completely stall communication, making them fail-stop failures[59].

In this paper, we focus on detecting fail-slow failures caused by core-level performance variance and link-level bandwidth degradation—both of which are prevalent and, more importantly, can propagate along communication and execution dependencies, leading to system slowdowns.

### 2.3 Performance Variance Modeling

Beside fail-slow failures, hardware performance has inherent variability[45]. To accurately capture the communication costs in many-core systems, we model those key performance parameters as random variables. Specifically, we model two main contributors to operation latency: computing capacity for cores and bandwidth for NoC.

Computing Capacity of each core, which affected by thermal pressure, throttling mechanism and so on, is assumed to follow a normal distribution [31, 53]. This distribution reflects the aggregated effect of microarchitectural factors such as clock frequency variation, temporary resource contention, and thermal-induced fluctuations, all of which tend to produce near-symmetric deviation around a nominal value. We denote the computing capacity  $P_{core} \sim N(\mu_c, \sigma_c^2)$  where  $\mu_c$  represents the expected processing capacity and  $\sigma_c^2$  quantifies the runtime variability.

**Bandwidth Fluctuation**. The latency associated with onchip interconnect links is subject to more asymmetric and bursty behavior, particularly under dynamic network load or in the presence of degraded hardware [28]. To model this, we adopt a Gamma distribution [45],  $T_{link} \sim Gamma(\alpha, \beta)$ , which provides flexibility in capturing latency variation caused by bandwidth. The shape parameter controls the burstiness of communication delays, while the rate parameter reflects average link throughput under contention. This distribution is particularly effective in approximating observed behaviors such as occasional long-tailed delays due to arbitration, flit contention, or rerouting in degraded paths.

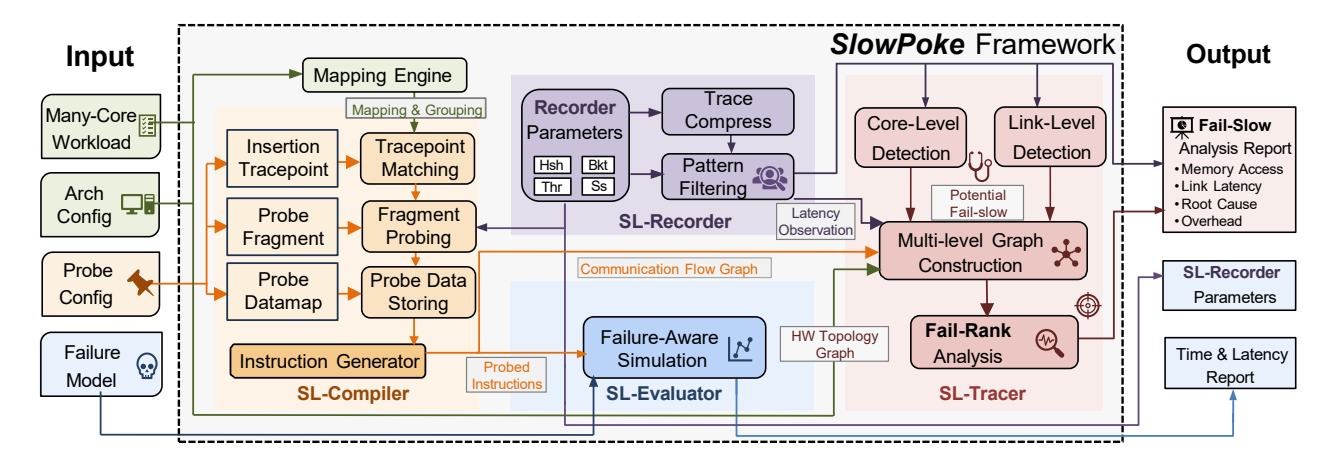


Figure 4. Overview of SlowPoke.

# 3 The SlowPoke Framework

SlowPoke is an automated framework for detecting and locating fail-slow failures in many-core systems. As shown in Figure 4, the framework is composed of three main components. **SL-Compiler** instruments the workload with lightweight probes, collecting runtime execution trace with minimal overhead. **SL-Recorder** then filters unrelevant trace and compresses redundant ones, producing a compact yet representative communication and execution patterns list. Finally, **SL-Tracer** leverages the compressed data to construct multilevel communication graph and perform FailRank algorithm on it, pinpointing fail-slow cores or links responsible for performance degradation. Together, these components form a systematic pipeline that bridges low-overhead monitoring with high-accuracy failures diagnosis.

#### 3.1 Input and Output

As shown in the left of Figure 4, the inputs to SlowPoke consist of: (1) Many-Core Workload: workloads are composed of basic I/O, communication, and compute instructions such as *read*, *recv*, and *conv*. The framework supports arbitrary task-to-core mappings [24, 35, 81]. In our implementation, we use a Gemini-like [7] mapping for evaluation; (2) Arch Config: the specification of target hardware architecture, which enables analysis across different many-core systems; (3) Probe Config: parameters that determine what data to collect, where to place probes, and how to store the collected traces data; (4) Failure Model: definitions of fail-slow behavior, including duration, degradation rate, and other settings.

Given these inputs, SlowPoke automatically generates probed instructions, collects runtime traces, and performs fail-slow analysis. The outputs fall into two categories: **fail-slow detection results**, including fail-slow root cause, SL-Recorder's optimal parameters, and the overhead of data collection and storage; and **system-level information**, such as total simulation time and execution latency.

## 3.2 SL-Compiler

This SL-Compiler takes workload mapping as input and is responsible for instrumenting program code with lightweight performance probes before execution. Inspired by the modular and event-driven design of eBPF (extended Berkeley Packet Filter), we decompose the monitoring process into three key abstractions. **Probe fragments** define what data to collect, **insertion tracepoints** specify where to place the probes, and **performance data maps** determine how to store the collected data. Figure 5 shows an example of SL-Compiler probing. The probed compute graph has detailed monitoring fragments without changing the program's logic or significantly affecting its runtime performance.

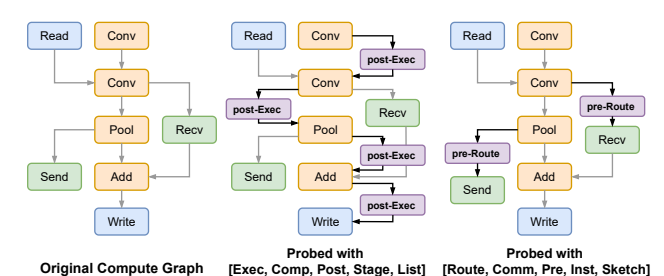


**Figure 5.** Examples of SL-Compiler probing.

The probe strategy is defined by a five-tuple. As summarized in Table 1, each abstraction is parameterized by several fine-grained components. Fragment controls the probe fragment; Type and Location jointly specify the insertion tracepoint; Level and Structure define the data map for managing collected traces. By adapting the core ideas of eBPF, we create a user-friendly and efficient monitoring mechanism tailored for many-core architectures.

**Probe fragment.** To collect performance data without disrupting program execution, we introduce the probe fragment, a lightweight pseudo-instruction. As shown in Table 1, fragments can capture computation-related events (Exec), communication activities (Route), or memory accesses (Mem). Figure 5b illustrates this case: by configuring Fragment=Exec,

**Table 1.** Components of probe's five-tuple definition.

Component	Option	Description	
Fragment	Exec Route Mem	Record calculation related traces Record communication traces Record memory access traces	
Туре	Comp Comm IO	Match compute instructions Match communication instructions Match input / output instructions	
Location	Pre Before the target instruction Post After the target instruction Surround Before & after the instruction		
Level	Inst Stage	Aggregate trace at instruction level Aggregate trace at stage level	
Structure	List Store traces in list manner Sketch Store traces using SL-Recorder		

probes are injected on compute instructions to record execution time. Similarly, Figure 5c shows the effect of setting Fragment=Route, which inserts probes on communication instructions to measure transmission latency. Crucially, these fragments do not interfere with the main compute pipeline, making them a portable tool for performance monitoring across different many-core systems.

Insertion tracepoint. To precisely control where fragments are placed, SL-Compiler introduces configurable insertion tracepoints, defined by Type (instruction filter) and Location (relative position), allowing flexible combination. As shown in Table 1, Type can be Comp, Comm, or IO to filter the target instruction type, while Location specifies whether the probe is anchored before, after, or surrounding the instruction. For example, by combining Type=Comp and Location=Post, Figure 5b insert probes after every compute instruction. These tracepoints are automatically inserted by SL-Compiler based on the static workload mapping, enabling complete monitoring coverage without manual work. Therefore, users can easily switch to different monitoring strategies to meet their needs.

Data map. Data collected by the probe fragments is stored in a performance data map, a highly configurable storage structure which balances precision and overhead. The map is parameterized by Level and Structure. The Level option controls aggregation granularity, from per-instruction (Inst) to per-stage (Stage), while the Structure option specifies storage organization. For example, we can use SL-Recorder (Sketch) for sparse data to save memory space and arrays (List) for dense data to provide fast access. To ensure low latency, these maps are initially stored in on-chip SRAM and are periodically offloaded to off-chip memory for long-running traces. Besides, by supporting incremental updates, eviction, and compression, these maps enable scalable trace management under different workload scales.

#### Algorithm 1: Fail-Slow Sketch Insertion **Input:** instruction trace *e*; number of hash tables *d*; number of buckets m; pattern threshold H**1 for** *each* $i \in [1, d]$ **do** $Index \leftarrow Hash(e.key) \mod m$ ; 3 $bucket \leftarrow HashTable[i][Index];$ if bucket.key equals to e.key then 4 5 increase the frequency of e by 1; if frequency of $e \ge H$ then Insert\_Stage\_2(e, 6 attributes); 7 else if bucket is empty then 8 $bucket.key \leftarrow e.key;$ 9 set the frequency of e to 1; 10 else decrease the frequency of e by 1; 11 12 **if** frequency of e is 0 **then** clear bucket to empty; 13 Function Insert\_Stage\_2(e, attr) 14 **if** *e.key* ∉ *Stage-2* **then** $\textbf{if } \textit{Stage-2.length} \geq \texttt{MAX\_LENGTH} \textbf{ then } \textbf{ evict the earliest}$ pattern in Stage-2; 16 insert e into Stage-2; 17 return 1; 18 19 Update(e.key, attr);

#### 3.3 SL-Recorder

return 0;

20

To reduce the storage overhead introduced by performance probes, we propose SL-Recorder, a lightweight on-the-fly data structure called the Fail-Slow Sketch, designed for trace compression and pattern-based filtering. As illustrated in Figure 6, the Fail-Slow Sketch operates in two stages. In Stage-1, a Running Track identifies frequently occurring traces with similar execution behaviors. In Stage-2, the common patterns among these traces are extracted, and their instance-specific information is aggregated based on shared patterns.

**Stage-1** consists of d of bucket arrays, each associated with a distinct hash function. These hash functions map trace features that characterize execution patterns to bucket indices, associating traces with similar behaviors to the same bucket. Each array contains m buckets, and each bucket has two fields: trace pattern (key) and its occurrence frequency. When the frequency exceeds a predefined threshold H, the corresponding trace pattern is considered a potential candidate for pattern extraction. Therefore, the threshold H directly controls the similarity of trace patterns, while the total number of buckets influences accuracy indirectly by limiting the number of candidate traces tracked at the same time.

**Stage-2** maintains a list of candidate fail-slow patterns and their associated attributes. This list supports operations such as updates and evictions, and its maximum length (MAX\_LENGTH) is determined based on the characteristics of

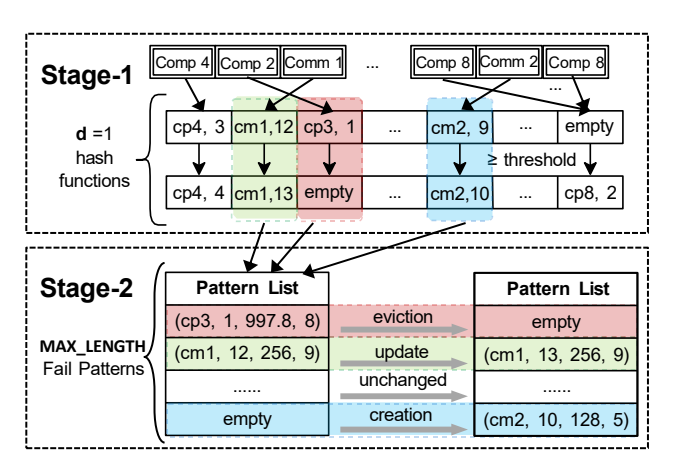


**Figure 6.** An example of Fail-Slow Sketch (d=1).

the workload. In this stage, traces with the same pattern are compressed, and statistical summaries of relevant performance metrics are computed to support root cause analysis. When the list reaches its maximum capacity, the Fail-Slow Sketch applies a First-In-First-Out (FIFO) replacement policy to make room for newly observed patterns.

**Insertion**. Given an input trace t, Fail-Slow Sketch first extracts its pattern features and computes the target bucket index using corresponding hash function. The trace is then inserted into the bucket (donated as b). As shown in Algorithm 1, there are three possible cases:

Case 1: t is not in the bucket, and b is currently empty. In this case, the trace pattern is stored in b, the frequency is set to 1, and the insertion completes.

Case 2: t is not in the bucket, and b is occupied. In this case, the frequency of b is decremented by 1. If the frequency drops to zero, the bucket is cleared, and the algorithm terminates.

Case 3: t is in the bucket b. In this case, the frequency counter is incremented by 1. If the frequency reaches the threshold H, the trace pattern is considered a candidate for Stage-2. If the pattern already exists in the Stage-2 list, its statistics are updated via update function; otherwise, a new pattern entry will be created. If the Stage-2 list has reached its capacity, typical replacement strategies such as frequencybased, probability-based, or arrival-time-based policies can be applied. In our design, we use an arrival-time-based replacement policy to ensure correct insertion of trace patterns. **Update**. Given a trace pattern and its attributes, the update operation modifies the corresponding entry in the Stage-2 pattern list to maintain the overall statistical information. For communication trace patterns, this includes updating metrics such as data volume and communication endpoints. For computation patterns, the update includes floating-point operation count, core id, and other relevant metrics. Additionally, all trace patterns have to maintain the timestamp of their first appearance and their duration, which are essential for localizing failure intervals during root cause analysis.

**Example**: Figure 6 shows a running example of Fail-Slow Sketch. To insert coming trace Comp4, Stage-1 extracts its pattern cp4. cp4 has been inserted into corresponding bucket before, so Fail-Slow Sketch adds the frequency of the bucket by 1 and finishes inserting. When inserting trace Comm2, the frequency of the bucket reaches threshold H=10 and there is space in Stage-2's pattern list. Therefore, Fail-Slow Sketch create a new trace pattern (cm2,10,128,5) for Comm2 through Creation operation, in which cm2 is the trace pattern, 10 is cm2's frequency, 128 is the data volume and 5 is the destination of communication. Besides, Fail-Slow Sketch performs Update operation for existing pattern cm1 and Eviction operation for deleted pattern cp3. After inserting all the traces, the compressed traces, also the trace patterns are stored in Stage-2's pattern list.

**Mathematical analysis**. It can be proven that increasing the number of hash functions d can effectively improve the retention probability, but also increases computational overhead; increasing the number of buckets m helps reduce hash collisions, but also increases storage overhead. We provide a proof for the conclusion as follow.

Given a fixed workload, let N be the number of instruction traces,  $f_i$  be the frequency of trace  $t_i$ ,  $B_j[k]$  be k-th bucket of j-th bucket array, and  $F_{i,j,k}$  be the number of traces mapped to bucket  $B_j[k]$  except for trace  $t_i$ .

LEMMA 3.1. For any trace pattern  $R_i$  in the instruction traces, let  $P(R_i)$  be its retention probability in Stage-2, then

$$P(R_i) \ge 1 - \left(\frac{N - f_i}{m(f_i - H)}\right)^d$$

PROOF. For a single bucket  $A_j[k]$  in Stage-1 which records trace  $t_i$ , according to the insertion algorithm, we have

$$f_i - F_{i,i,k} \leq A_i[k]. freq \leq f_i$$

Since the hash function is uniformly distributed, the probability of mapping to a specific bucket is  $\frac{1}{m}$ , so the expectation of  $F_{i,j,k}$  is

$$E[F_{i,j,k}] = \sum_{t \neq t_i} f_t \frac{1}{m} = \frac{N - f_i}{m}$$

For a trace pattern  $R_i$  in Stage-2 and threshold H, there must be a  $j \in \{1, 2, ..., d\}$  such that

$$f_i - F_{i,j,k} \ge H \Leftrightarrow F_{i,j,k} \le f_i - H$$

By Markov inequality, we can evaluate the probability of not recoding trace pattern  $R_i$  with one hash function

$$P(F_{i,j,k} \ge f_i - H) \le \frac{E[F_{i,j,k}]}{f_i - H} = \frac{N - f_i}{m(f_i - H)}$$

Since we have d hash functions, so the retention probability of a trace pattern  $R_i$  is

$$P(R_i) \geq 1 - (\frac{N - f_i}{m(f_i - H)})^d$$

We further conduct parameter sensitivity analysis (Section 4.4) and design space exploration (Section 4.5) to determine the optimal configuration of SL-Recorder.

#### 3.4 SL-Tracer

SL-Tracer is designed to identify and localize fail-slow failures across both computation and communication resources. It follows a detection–construction–analysis pipeline. First, core-level detection and link-level detection are performed to identify potential fail-slow candidates at different stages of the system. These candidates, together with the work-load's communication dependency graph and the hardware topology, are integrated in the multi-level graph construction stage. The resulting graph captures both structural relationships and performance anomalies. Finally, the FailRank algorithm operates on this graph to quantify the likelihood of each candidate being the root cause, providing a ranked explanation of fail-slow components.

**3.4.1 Core-Level Fail-Slow Detection.** The goal of corelevel fail-slow detection is to identify candidate cores that exhibit abnormal slowdowns compared to their peers. Our method targets for structured parallel applications and performs this detection in a stage-aware manner, leveraging the mapping from workload to many-core architecture.

As illustrated in Figure 7, we first partition computation instructions by execution stage (e.g., network layers, loop iterations, or pipeline segments), ensuring that only tasks with comparable semantics are grouped together. Next, cores are clustered according to the workload-to-core mapping. Each group therefore contains functionally equivalent computations executed across different cores, making their performance directly comparable.

Within each group, we measure the performance of each core in terms of floating-point operations (FLOPs) per unit time. The group average serves as the baseline, and we perform outlier detection to highlight cores whose FLOPs are significantly lower than the baseline. These outliers are flagged as fail-slow candidates. For example, in Figure 7, core 6 and 10 deviate from their group peers and are thus marked as candidates. Each candidate is further assigned a fail-slow probability, derived from the normal distribution of its performance variance. This probability is then used as the initial fail-slow score for the FailRank algorithm (Sec 3.4.3).

To further localize fail-slow behavior, we maintain the start and end timestamps of each instruction. This temporal information reveals the intervals during which a slowdown exists, offering fine-grained visibility into the occurrence and persistence of fail-slow failure and enabling correlation between localized anomalies and downstream abnormal behaviors.

**3.4.2 Link-Level Fail-Slow Detection.** The goal of the link-level fail-slow detection module is to identify interconnect links that exhibit abnormal bandwidth degradation

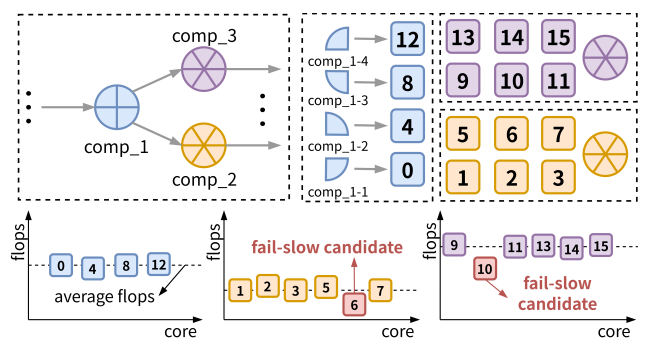


Figure 7. Core level fail-slow detection.

during program execution. Since such fail-slow behaviors cannot be directly observed under limited hardware visibility, we infer them from communication traces collected by SL-Recorder. Specifically, we formulate the problem as a statistical inference task, where observed end-to-end communication delays are decomposed to estimate the bandwidth of individual links.

For each communication event extracted from execution traces, we record four key attributes: the transferred data volume, the measured transmission time, and the index of the source and destination cores. Leveraging the deterministic routing algorithm of the 2D-mesh interconnect, we map each event to the set of links traversed along its multi-hop path, thereby associating observed end-to-end latency with individual link bandwidths.

To estimate link bandwidth, we transform the problem into a set of linear equations by turning each link's bandwidth  $b_i$  into its inverse  $\theta_i = \frac{1}{b_i}$ . Each communication event yields an equation of the form  $Ax^T = T_{comm}$ , where A represents the link composition of paths, x represents  $\theta_i$  vector and  $T_{comm}$  represents the observed transmission times.

Because the system is underdetermined and affected by measurement noise, we adopt the Expectation–Maximization (EM) algorithm to infer link bandwidths. EM algorithm iteratively estimates link bandwidths by alternating between (1) computing expected path-level delays given current bandwidth estimates and (2) updating bandwidth estimates to maximize the likelihood of the observed traces. This process converges to a set of link bandwidths that best explain the data, even under partial or noisy observations.

3.4.3 Fail-Slow Root Cause Analysis. To localize fail-slow root causes in many-core systems, we construct a multi-level communication graph that integrates hardware topology, execution dependencies, and runtime tracing data. This augmented graph captures how performance degradation propagates across cores and links, turning the localization into a graph-based inference problem. On this foundation, we design FailRank, a PageRank-inspired algorithm that quantifies the propagation path of fail-slows, enabling accurate root cause identification.

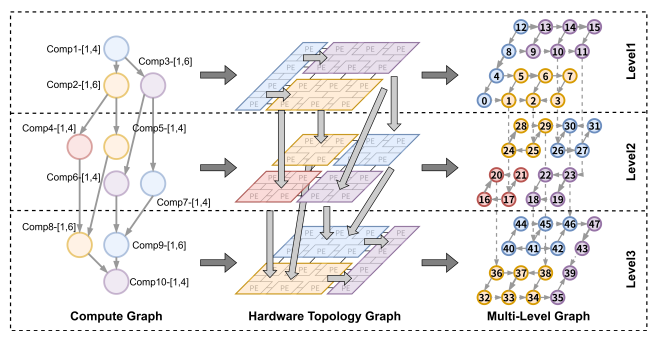


Figure 8. Construction of multi-level communication graph.

**Multi-Level Communication Graph.** We define the Multi-Level Communication Graph (MCG) as a layered graph G = (V, E) that integrates execution dependency and hardware topology, shown in the right of Figure 8. Each node  $v \in V$  represents a core at a specific time window, bounded with a set of computation instructions. The likelihood for being root cause of node v is quantified by a fail-slow score  $s(v) \in [0,1]$  (determined in Sec 3.4.1). Each directed edge  $e = (u,v) \in E$  denotes communication dependency between two cores, bounded with a set of communication instructions. The edge is associated with a propagation weight w(u,v), capturing the probability that performance degradation propagates from core u to v.

To construct the MCG, we perform a depth-first search (DFS) on the workload's computation graph  $G_c = (V_c, E_c)$ . As illustrated in Figure 8,  $G_c$  is a directed acyclic graph (DAG). For each dependency edge  $(x,y) \in E_c$ , we first determine the physical cores p(x) and p(y) assigned to tasks x and y. The mapping  $p:V_c \to E_h$  links computation nodes to hardware cores in the hardware topology  $G_h = (V_h, E_h)$ . The communication path between p(x) and p(y) is the identified as a sequence of hardware links  $\{e_1, e_2, ..., e_k\} \in E_h$ . For each traversed link  $e_i$ , we increment its traffic volume  $T(e_i)$  by the transported data size of (x, y).

After traversing the entire DAG, we normalize the traffic volumes to derive edge propagation weights. Specifically, for each core  $u \in V_h$ , let  $Out(u) = \{(u,v) \in E_h\}$  denote its outgoing links. This normalization ensures that  $\Sigma_{(u,v')\in Out(u)}w(u,v')=1$ , making w(u,v) interpretable as the probability of failure propagation through link (u,v). The resulting MCG thus provides a structured, probabilistic view of how fail-slow behaviors may spread across both computation and communication dependency within a level.

To capture cross-level interactions, we introduce virtual DRAM nodes that connect levels. These nodes represent interactions through memory, such as fetches or writes between different levels. Edges connected to a DRAM node represent inter-level dependencies, showing how fail-slow may propagate across levels. This vertical connection adds a temporal dimension to MCG, allowing the FailRank algorithm to analyze the timing and causality of fail-slows.

FailRank Algorithm. To localize fail-slow root causes from core-level and link-level candidates, we propose FailRank, a graph-based iteration algorithm inspired by PageRank, which identifies fail-slow root causes on MCG. Unlike PageRank that only updates node scores based on their neighbors with uniform transition probabilities, FailRank incorporates propagation weights of their neighbor links.

The algorithm initialize fail-slow scores with the probabilities obtained in core-level and link-level detection, denoted as  $s_0(v)$  for node v and  $l_0(u,v)$  for edge (u,v). At each iteration, a node's score is updated not only from its neighboring nodes but also from the weighted contributions of connecting links:

$$s^{(k+1)}(v) = (1-\lambda)s_0(v) + \lambda \sum_{(u,v) \in F} w(u,v)s^{(k)}(u)$$

where w(u, v) is the normalized propagation weight of edge (u, v) defined in Sec 3.4.2. Each link's score is updated after iteration by combining three factors: the propagation weight, the fail-slow scores of its endpoint node u, and its current score:

$$l^{(k+1)}(u,v) = \alpha w(u,v) + \beta s^{(k)}(u) + \gamma l^{(k)}(u,v)$$

where  $\alpha$ ,  $\beta$ ,  $\gamma$  are workload-dependent coefficients. Users can flexibly tune the edge update weights according to workload characteristics—for instance, setting a higher  $\alpha$  for applications with intensive communication request. In our experiments, we set  $\alpha = 0.1$ ,  $\beta = 0.3$ ,  $\gamma = 0.6$ .

As Figure 9 shows, FailRank starts with initial fail-slow candidates and iteratively updates their scores until convergence. Each node is assigned a fail-slow score s, as annotated in the figure (e.g., s = 0.8, 0.7), which reflects the likelihood of being the root cause. Edges indicate communications between cores. Red edge has higher communication volume, while the dashed edge shows memory-access dependencies between levels. During iterations, the nodes with higher fail-slow scores and edges with heavier traffic exert stronger influence on their neighbors. After convergence, FailRank normalizes node and edge scores within each level of the MCG using a softmax function, yielding a probability distribution that pinpoints the most likely fail-slow root cause.

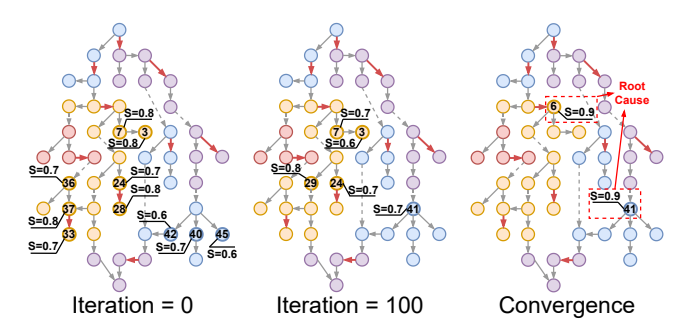


Figure 9. An example of FailRank algorithm.

## 3.5 Implementation

We implement SlowPoke simulator with SimPy[47], which enables event-driven modeling of concurrent events, resource contention, and time-dependent interactions across thousands of processes[79]. The many-core architecture, including cores, interconnects, and memory hierarchies, is represented as SimPy processes, allowing us to capture instruction traces, probe execution, and data movement for accurate modeling of fail-slow propagation. To evaluate failure scenarios, the simulator employs a monitoring-process-based injection mechanism: user-specified configurations are read at initialization, and during execution, a dedicated monitoring process dynamically alters the performance parameters of target components to emulate fail-slow behavior, automatically restoring them once the failure ends.

#### 4 Evaluation

# 4.1 Experimental Setup

Evaluated Workloads. We construct a binary tree compute graph and calculate matrix operations on each node as a micro-benchmark. Besides, we evaluate SlowPoke on four representative neural networks, including GoogLeNet[58], DarkNet-19[52], VGG[56], and ResNet-50[25]. These workloads cover a range of computational and communication patterns, providing a comprehensive testbed for fail-slow detection. As mentioned in Sec 3.1, the workload mappings are generated using the Gemini[7] framework or following its style, which describes the tensor partition and block mapping clearly.

**Fail-Slow Dataset.** To evaluate the accuracy of fail-slow detection, we construct a dataset consisting of 152 fail-slow failure instances that capture diverse failure modes. Each failure is characterized by three parameters: failure location, duration, and slowdown rate. The dataset includes two types of failure locations—core-level and link-level—with an approximate ratio of 7:3. Failure durations are uniformly distributed between 0 s and 10 s, while the slowdown rate is fixed at 10× to ensure consistent severity across cases.

For different workloads, failures are reused as long as they can affect workload execution; failures that take place on unused resources are excluded. For different hardware architectures, additional failures are constructed to reflect the larger set of possible failure locations (4×4, 6×6, 8×8) in larger-scale systems. To ensure a balanced evaluation, we also construct an equal number of negative samples by modifying DNN structures to generate workloads without fail-slow failures. This dataset provides a controlled yet diverse set of fail-slow scenarios, enabling comprehensive evaluation of SLOTH in terms of detection accuracy, root cause localization, and robustness across workloads and architectures.

**Baseline.** To better evaluate the effectiveness of SlowPoke, we compare it with two baseline tracing approaches:

**Table 2.** Fail-slow detection accuracy.

Algorithm	Workload	Accuracy↑(%)	FPR↓(%)
	DarkNet-19	50.92(138/271)	53.29(81/152)
	GoogLeNet	51.65(141/273)	54.61(83/152)
Threshold	VGG	45.45(125/275)	59.09(91/154)
	ResNet-50	51.29(139/271)	56.77(88/155)
	Binary Tree	60.44(165/273)	46.05(70/152)
	DarkNet-19	68.20(193/283)	33.97(53/156)
	GoogLeNet	67.14(188/280)	37.58(59/157)
Microscope	VGG	68.46(191/279)	35.26(55/156)
	ResNet-50	64.47(176/273)	45.22(71/157)
	Binary Tree	79.20(217/274)	23.75(38/160)
	DarkNet-19	80.40(242/301)	12.64(22/174)
	GoogLeNet	88.30(264/299)	13.64(24/176)
SlowPoke (Ours)	VGG	87.38(263/301)	14.61(26/178)
	ResNet-50	82.79(255/308)	16.48(30/182)
	Binary Tree	94.98(265/279)	3.18(5/157)

(1) **Threshold Filtering**: We implement a threshold based fail-slow detection method that directly analyzes the raw trace data collected during workload execution. This approach monitors key performance indicators such as computation time and communication latency, and flags a component as fail-slow if its metric exceeds a predefined threshold.

(2) **Modified Microscope** [38]: This method uses directed acyclic graphs to represent the dependency among microservices, identifying and locating the abnormal services with a ranked list of possible root causes. We modified it to detect fail-slow failures.

#### 4.2 Fail-slow Root Cause Detection

We evaluate SlowPoke's effectiveness of fail-slow root cause detection across 5 workloads. As shown in Table 2, both Threshold Filtering and Microscop have low detection accuracy and high False-Positive Rate (FPR), indicating that they are not good at localizaing fail-slow root cause. In contrast, SlowPoke achieves consistently high accuracy, ranging from 80.4% to 94.98%. Among them, binary tree demonstrates the best performance, with 94.98% accuracy and a low FPR of 3.18%. The reason is the binary tree computation graph is structurally simple, making fail-slow attribution more reliable.

However, DarkNet-19 exhibits a relatively low accuracy (80.4%). The main reason lies in its uniform workload mapping pattern, which produces highly correlated traces. This correlation increases the estimation error of the EM-based inference, resulting in many undetected fail-slows. Other DNN workloads, such as GoogLeNet, VGG, and ResNet-50, fall between these two extremes, with accuracy around 83–88% and moderate error rates. Compared to DarkNet-19, these models benefit from more diverse communication patterns, which provide richer trace information for inference.

Overall, these results demonstrate that SlowPoke can achieve effective fail-slow root cause detection across different workloads, while its accuracy is influenced by workload structure and trace diversity.

#### 4.3 Data Collection Overhead

In this experiment, we evaluate the runtime overhead introduced by the proposed probe-based data collection mechanism. We simulate the execution of DarkNet-19, ResNet-50, GoogLeNet, VGG and Binary Tree workloads under different probe configurations. In the simulator, the latency of a probe is determined by the amount of data it collects. For example, retrieving the current system clock incurs a 10-cycles delay. We use the total execution time without any probes as the baseline. The Communication Probe, Computation Probe, and Full Probe configurations correspond to inserting probes into communication instructions, computation instructions, and all instructions, respectively, in order to assess the overhead in different analysis scenarios. Considering the variability in hardware performance, we repeat the experiments multiple times under the same configuration and report the average execution time as the measured

Figure 10 shows that our probe-based data collection mechanism gathers runtime traces with low overhead. Even in the most intrusive configuration, where probes are inserted into all instructions, the execution time increases by at most 10% compared to the baseline. For more targeted scenarios, (e.g., Communication Probe for network performance monitoring), the overhead remains below 5%.

#### 4.4 Effectiveness of Storage Overhead Reduction

In this experiment, we evaluate the storage effectiveness of SL-Recorder in reducing the storage overhead of trace data through compression. We use the five workloads mentioned before to measure the memory consumption of trace data under both raw and compressed formats. The raw data records most of the information such as index, timestamps and operands of an instruction, and is considered as the baseline. For each workload, we separately record the storage overhead of communication-related traces and computation-related traces, and then apply SL-Recorder's compression mechanism to obtain the reduced storage cost. We compare the total memory consumption before and after compression to quantify the storage saving achieved by SL-Recorder.

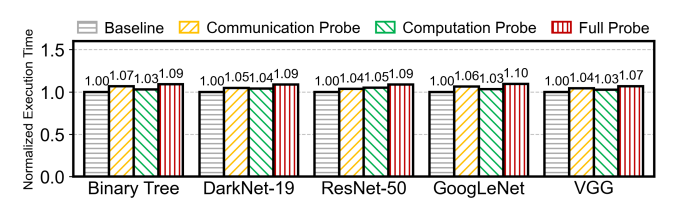


**Figure 10.** Time overhead of SL-Compiler probing.

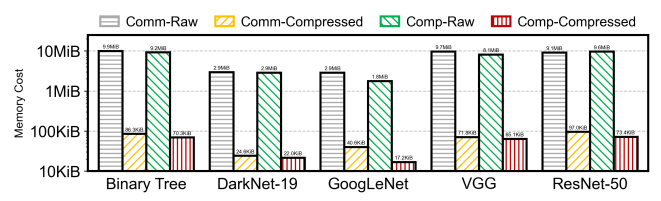
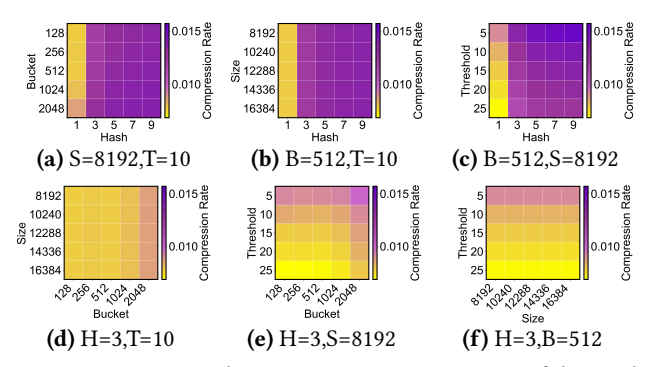


Figure 11. Memory cost of communication and computation traces with and without SL-Recorder.



**Figure 12.** SL-Recorder compression rate: Impact of the Hash (H), Bucket (B), Size (S), and Threshold (T).

Figure 11 shows the memory cost of raw and compressed traces across different workloads. In this figure, Comm represent the memory required for communication and Comp represent that of computation traces, respectively. We observe that SL-Recorder achieves substantial storage reduction and is effective across workloads of different scales. For small-scale workloads such as DarkNet-19, SL-Recorder reduces the storage overhead to 0.8% and 0.7% of the original sizes for communication and computation traces, respectively. Even for large-scale workloads such as VGG, SL-Recorder maintains a similar compression ratio, reducing a total of approximately 17.8 MiB of trace data to only 137.2 KiB. Overall, these results demonstrate that SL-Recorder can reduce storage overhead by more than two orders of magnitude, significantly lowering memory requirements.

Further, we examine how the internal parameters of SL-Recorder influence its compression efficiency. We conduct this experiment on DarkNet-19, varying four parameters: the number of hash functions (Hash, H), the number of buckets (Bucket, B), the Stage-2 size (Size, S), and the pattern-selection threshold (Threshold, T). To capture the interaction effects between parameters, we fix two of them at default values and vary the other two, measuring the resulting compression ratio. The results are visualized using heatmaps, where each heatmap illustrates how the compression ratio changes under different parameter combinations.

Figure 12 illustrates the impact of different parameter settings on the compression ratio of SL-Recorder. Among the four parameters, H, B, and T show a clear influence on compression effectiveness, while S has little impact. Specifically, a smaller number of hash functions and buckets, as well as

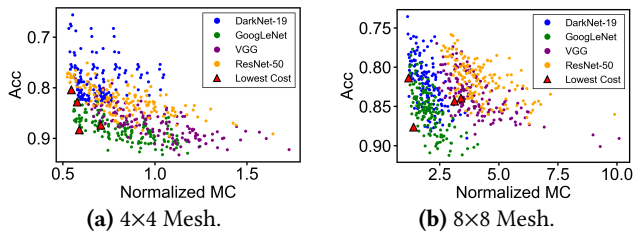


Figure 13. SL-Recorder Design Space Exploration.

a larger threshold, consistently lead to stronger compression. In contrast, varying S across a wide range does not significantly alter the compression ratio, indicating that this parameter is relatively insensitive. These observations suggest that tuning hash, bucket, and threshold values is crucial for achieving high compression efficiency, whereas Stage-2 size can be fixed without noticeably affecting performance.

# 4.5 Design Space Exploration

To find out the optimal configuration of SL-Recorder, we conduct a design space exploration (DSE) across four key parameters: the number of hash functions (Hash), the number of buckets (Bucket), the Stage-2 size (Size), and the pattern-selection threshold (Threshold). These parameters jointly determine the compression efficiency and detection accuracy of SL-Recorder.

We define a composite optimization objective as:  $COST = ACC^{\alpha} \times R^{\beta} \times M^{\gamma}$ , where ACC represents the detection accuracy, R denotes the data compression rate, and M refers to the memory overhead of data structure. By adjusting the hyperparameters  $\alpha$ ,  $\beta$ ,  $\gamma$ , users can flexibly prioritize accuracy, compression rate, or memory overhead according to their own deployment requirements. Here we set  $\alpha = -1$ ,  $\beta = \gamma = 1$ , considering all three objectives equally.

Figure 13a shows the exploration results on a 4×4 many-core architecture, where each point corresponds to a parameter configuration, and different colors represent different workloads. We can observe that the design space exhibits clear trade-offs: configurations with lower memory cost often suffer from degraded accuracy, whereas moderate-cost configurations yield balanced performance. The lowest-cost Pareto-optimal cases are highlighted with red triangles. Figure 13b shows DSE results on a 8×8 many-core architecture, which has the same trade-off like 4×4 architecture.

### 4.6 Scalability Analysis

To evaluate the scalability of SlowPoke, we test its performance on many-core architectures of increasing scale. Specifically, we simulate ResNet-50 and DarkNet-19 on  $4\times4$ ,  $6\times6$ , and  $8\times8$  architectures, and measure the execution time under three probing modes: communication probe, computation probe, and full probe.

The results are shown in Figure 14. For both networks, the overall execution time decreases as the architecture scale grows, which indicates that larger many-core systems provide higher parallelism and better workload distribution. More importantly, the additional overhead introduced by probing remains consistently low across different scales. As illustrated by the green points in the figure, the normalized execution time overhead of the full probe is always below 10%, demonstrating that our framework introduces only marginal overhead even at larger scales.

Figure 15 further evaluates memory efficiency and detection accuracy. As the scale increases, the volume of trace data naturally grows, resulting in higher raw memory cost. However, SL-Recorder consistently achieves nearly 100× reduction in memory consumption across different scales, showing that the compression ratio is insensitive to architecture scale. Meanwhile, the detection accuracy of fail-slow faults remains stable, with only minor fluctuations and no significant degradation as the architecture grows.

# 5 Related Work

Distributed tracing and storage. Prior studies reduce tracing overhead through selective collection and compact storage. Mint [29] and Pivot Tracing [44] lower cost via commonality analysis and dynamic causal monitoring, while Hindsight [78] and Sieve [30] apply selective tracing and attention-based sampling. Lightweight sketches such as Dynamic Sketch [68] and Stable-Sketch [36] offer compact representations for stream data. However, these methods generally preserve high-frequency items statically once stored. In contrast, our SL-Recorder adaptively updates patterns and retains traces most relevant to fail-slow behaviors.

**Performance failure detection**. Many works have analyzed hardware-induced performance variance in large-scale systems. ScalAna [32] and What-if Analysis [39] employ graph analysis for bottlenecks, while vSensor [60] and Vapro

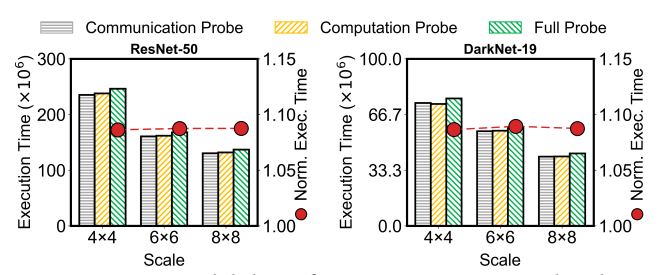
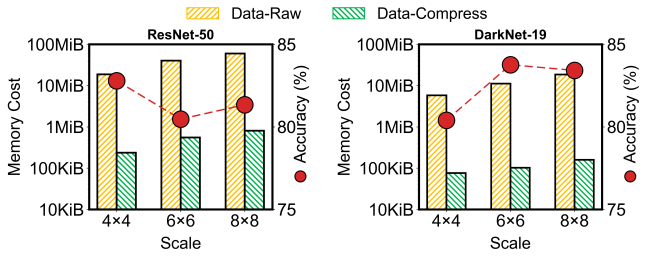


Figure 14. Scalability of SlowPoke: Time overhead.



**Figure 15.** Scalability of SlowPoke: Memory cost and detection accuracy.

[82] use workload snippets to detect fluctuations. Profiling-based tools like Scalasca [69] and GVARP [75] also target variance in parallel applications. Recent systems, e.g., FAL-CON [70], isolate stragglers in cloud and training workloads. However, these methods assume abundant storage, which is not suitable for on-chip environments. Our SL-Tracer works under strict memory limits while pinpointing fail-slow components.

Root cause analysis. Root cause analysis (RCA) often leverages structured traces and graph models for localization. Event-graph approaches like Groot [64] and GNN-based Sleuth [20] capture causal anomalies, while Sage [19] and MicroRank [76] apply spectrum analysis and performance metrics. Systems such as IASO [49] and TraceRCA [37] detect fail-slow symptoms in distributed services. However, these works focus on communication dependencies, overlooking hardware topology. Our SL-Tracer unifies both communication and hardware structures for more accurate fail-slow root cause localization.

# 6 Conclusion

In this work, we introduce SlowPoke, a tracing and analyzing framework for detecting and localizing fail-slow failures in many-core systems. SlowPoke provides a full-stack solution that spans lightweight data collection, online trace compression, and graph-based root cause analysis. Specifically, we design SL-Compiler to insert low-overhead tracing probes into the target workload, SL-Recorder to achieve runtime trace filtering and compression, and SL-Tracer for accurate fail-slow localization. We evaluate SlowPoke using a set of representative workloads and hardware configurations. Experiments demonstrate the effectiveness of SlowPoke. It reduces the storage overhead of detection traces by an average of 115.9x, while achieving an average fail-slow detection accuracy of 86.77% with an FPR of 12.11%. These results highlight the practicality of SlowPoke and its capability to provide scalable fail-slow detection across diverse many-core architectures.

# References

- Mridul Agarwal, Bipul C Paul, Ming Zhang, and Subhasish Mitra. 2007.
   Circuit failure prediction and its application to transistor aging. In 25th IEEE VLSI Test Symposium (VTS'07). IEEE, IEEE, Berkeley, CA, USA, 277–286.
- [2] Armin Ahmadzadeh and Hamid Sarbazi-Azad. 2023. Fast and scalable quantum computing simulation on multi-core and many-core platforms. Quantum Information Processing 22 (05 2023). doi:10.1007/ s11128-023-03955-w
- [3] Ramnatthan Alagappan, Aishwarya Ganesan, Yuvraj Patel, Thanumalayan Sankaranarayana Pillai, Andrea C Arpaci-Dusseau, and Remzi H Arpaci-Dusseau. 2016. Correlated crash vulnerabilities. In 12th USENIX Symposium on Operating Systems Design and Implementation (OSDI 16). USENIX Association, Savannah, GA, USA, 151–167.
- [4] Rajeshwari Banakar, Stefan Steinke, Bo-Sik Lee, Mahesh Balakrishnan, and Peter Marwedel. 2002. Scratchpad memory: design alternative for cache on-chip memory in embedded systems. In *Proceedings of the*

- tenth international symposium on Hardware/software codesign. ACM, Estes Park, Colorado, USA, 73–78.
- [5] Kshitij Bhardwaj, Koushik Chakraborty, and Sanghamitra Roy. 2012. Towards graceful aging degradation in NoCs through an adaptive routing algorithm. In Proceedings of the 49th Annual Design Automation Conference. ACM, San Francisco, California USA, 382–391.
- [6] Tobias Bjerregaard and Shankar Mahadevan. 2006. A survey of research and practices of network-on-chip. ACM Computing Surveys (CSUR) 38, 1 (2006), 1-es.
- [7] Jingwei Cai, Zuotong Wu, Sen Peng, Yuchen Wei, Zhanhong Tan, Guiming Shi, Mingyu Gao, and Kaisheng Ma. 2024. Gemini: Mapping and architecture co-exploration for large-scale dnn chiplet accelerators. In 2024 IEEE International Symposium on High-Performance Computer Architecture (HPCA). IEEE, IEEE, Edinburgh, United Kingdom, 156– 171
- [8] Yung-Chang Chang, Ching-Te Chiu, Shih-Yin Lin, and Chung-Kai Liu. 2011. On the design and analysis of fault tolerant NoC architecture using spare routers. In 16th Asia and South Pacific Design Automation Conference (ASP-DAC 2011). IEEE, IEEE, Yokohama, Japan, 431–436.
- [9] Yu-Hsin Chen, Joel Emer, and Vivienne Sze. 2016. Eyeriss: A spatial architecture for energy-efficient dataflow for convolutional neural networks. ACM SIGARCH computer architecture news 44, 3 (2016), 367–379.
- [10] Allen Clement, Edmund Wong, Lorenzo Alvisi, Mike Dahlin, Mirco Marchetti, et al. 2009. Making Byzantine fault tolerant systems tolerate Byzantine faults. In Proceedings of the 6th USENIX symposium on Networked systems design and implementation. The USENIX Association, USENIX Association, Boston, MA, 153–168.
- [11] Guojing Cong and Konstantin Makarychev. 2012. Optimizing Large-scale Graph Analysis on Multithreaded, Multicore Platforms. In 2012 IEEE 26th International Parallel and Distributed Processing Symposium. IEEE, Shanghai, China, 414–425. doi:10.1109/IPDPS.2012.46
- [12] Jack B Dennis and David P Misunas. 1974. A preliminary architecture for a basic data-flow processor. In *Proceedings of the 2nd annual symposium on Computer architecture*. ACM, Barcelona, Spain, 126–132.
- [13] Pratyush Dhingra, Jana Doppa, and Partha Pratim Pande. 2024. HeTraX: Energy Efficient 3D Heterogeneous Manycore Architecture for Transformer Acceleration. In Proceedings of the 29th ACM/IEEE International Symposium on Low Power Electronics and Design (Newport Beach, CA, USA) (ISLPED '24). Association for Computing Machinery, New York, NY, USA, 1–6. doi:10.1145/3665314.3670814
- [14] Pratyush Dhingra, Janardhan Rao Doppa, and Partha Pratim Pande. 2025. Atleus: Accelerating Transformers on the Edge Enabled by 3D Heterogeneous Manycore Architectures. *IEEE Transactions on Computer-Aided Design of Integrated Circuits and Systems* 44, 8 (2025), 2842–2855. doi:10.1109/TCAD.2025.3531255
- [15] Bernhard Egger, Jaejin Lee, and Heonshik Shin. 2006. Scratchpad memory management for portable systems with a memory management unit. In Proceedings of the 6th ACM & IEEE International Conference on Embedded Software (Seoul, Korea) (EMSOFT '06). Association for Computing Machinery, New York, NY, USA, 321–330. doi:10.1145/1176887.1176933
- [16] Stijn Eyerman, Wim Heirman, Kristof Du Bois, Joshua B. Fryman, and Ibrahim Hur. 2018. Many-Core Graph Workload Analysis. In SC18: International Conference for High Performance Computing, Networking, Storage and Analysis. IEEE, Texas, Dallas, 282–292. doi:10.1109/SC. 2018.00025
- [17] Yinxiao Feng, Wei Li, and Kaisheng Ma. 2024. Ring Road: A Scalable Polar-Coordinate-based 2D Network-on-Chip Architecture. In 2024 57th IEEE/ACM International Symposium on Microarchitecture (MICRO). IEEE, IEEE, Austin, TX, USA, 871–884.
- [18] Yinxiao Feng, Dong Xiang, and Kaisheng Ma. 2023. A scalable methodology for designing efficient interconnection network of chiplets. In 2023 IEEE International Symposium on High-Performance Computer

- Architecture (HPCA). IEEE, IEEE, Montreal, OC, Canada, 1059-1071.
- [19] Yu Gan, Mingyu Liang, Sundar Dev, David Lo, and Christina Delimitrou. 2021. Sage: practical and scalable ML-driven performance debugging in microservices. In Proceedings of the 26th ACM International Conference on Architectural Support for Programming Languages and Operating Systems (Virtual, USA) (ASPLOS '21). Association for Computing Machinery, New York, NY, USA, 135–151. doi:10.1145/3445814.3446700
- [20] Yu Gan, Guiyang Liu, Xin Zhang, Qi Zhou, Jiesheng Wu, and Jiangwei Jiang. 2024. Sleuth: A Trace-Based Root Cause Analysis System for Large-Scale Microservices with Graph Neural Networks. In Proceedings of the 28th ACM International Conference on Architectural Support for Programming Languages and Operating Systems, Volume 4 (Vancouver, BC, Canada) (ASPLOS '23). Association for Computing Machinery, New York, NY, USA, 324–337. doi:10.1145/3623278.3624758
- [21] Paul Gratz, Changkyu Kim, Robert McDonald, Stephen W Keckler, and Doug Burger. 2006. Implementation and evaluation of on-chip network architectures. In 2006 International Conference on Computer Design. IEEE, IEEE, San Jose, CA, USA, 477–484.
- [22] Haryadi S Gunawi, Riza O Suminto, Russell Sears, Casey Golliher, Swaminathan Sundararaman, Xing Lin, Tim Emami, Weiguang Sheng, Nematollah Bidokhti, Caitie McCaffrey, et al. 2018. Fail-slow at scale: Evidence of hardware performance faults in large production systems. ACM Transactions on Storage (TOS) 14, 3 (2018), 1–26.
- [23] Mohammad-Hashem Haghbayan, Antonio Miele, Zhuo Zou, Hannu Tenhunen, and Juha Plosila. 2020. Thermal-cycling-aware dynamic reliability management in many-core system-on-chip. In 2020 Design, Automation & Test in Europe Conference & Exhibition (DATE). IEEE, IEEE, Grenoble, France, 1229–1234.
- [24] Edward Hanson, Shiyu Li, Guanglei Zhou, Feng Cheng, Yitu Wang, Rohan Bose, Hai Li, and Yiran Chen. 2023. Si-kintsugi: Towards recovering golden-like performance of defective many-core spatial architectures for ai. In *Proceedings of the 56th Annual IEEE/ACM International Symposium on Microarchitecture*. ACM, ON, Toronto, Canada, 972–985.
- [25] Kaiming He, Xiangyu Zhang, Shaoqing Ren, and Jian Sun. 2016. Deep Residual Learning for Image Recognition. In 2016 IEEE Conference on Computer Vision and Pattern Recognition (CVPR). IEEE, Las Vegas, NV, USA, 770–778. doi:10.1109/CVPR.2016.90
- [26] Yi He, Mike Hutton, Steven Chan, Robert De Gruijl, Rama Govindaraju, Nishant Patil, and Yanjing Li. 2023. Understanding and mitigating hardware failures in deep learning training systems. In *Proceedings* of the 50th Annual International Symposium on Computer Architecture. ACM, FL, Orlando, USA, 1–16.
- [27] Kartik Hegde, Po-An Tsai, Sitao Huang, Vikas Chandra, Angshuman Parashar, and Christopher W Fletcher. 2021. Mind mappings: enabling efficient algorithm-accelerator mapping space search. In Proceedings of the 26th ACM International Conference on Architectural Support for Programming Languages and Operating Systems. ACM, Virtual, USA, 943–958.
- [28] Carles Hernández, Federico Silla, and José Duato. 2010. A methodology for the characterization of process variation in NoC links. In 2010 Design, Automation & Test in Europe Conference & Exhibition (DATE 2010). IEEE, IEEE, Dresden, Germany, 685–690.
- [29] Haiyu Huang, Cheng Chen, Kunyi Chen, Pengfei Chen, Guangba Yu, Zilong He, Yilun Wang, Huxing Zhang, and Qi Zhou. 2025. Mint: Cost-Efficient Tracing with All Requests Collection via Commonality and Variability Analysis. In Proceedings of the 30th ACM International Conference on Architectural Support for Programming Languages and Operating Systems, Volume 1 (Rotterdam, Netherlands) (ASPLOS '25). Association for Computing Machinery, New York, NY, USA, 683–697. doi:10.1145/3669940.3707287
- [30] Zicheng Huang, Pengfei Chen, Guangba Yu, Hongyang Chen, and Zibin Zheng. 2021. Sieve: Attention-based Sampling of End-to-End Trace Data in Distributed Microservice Systems. In 2021 IEEE International Conference on Web Services (ICWS). IEEE, Chicago, IL, USA,

- 436-446. doi:10.1109/ICWS53863.2021.00063
- [31] Yuichi Inadomi, Tapasya Patki, Koji Inoue, Mutsumi Aoyagi, Barry Rountree, Martin Schulz, David Lowenthal, Yasutaka Wada, Keiichiro Fukazawa, Masatsugu Ueda, et al. 2015. Analyzing and mitigating the impact of manufacturing variability in power-constrained supercomputing. In Proceedings of the international conference for high performance computing, networking, storage and analysis. ACM, Texas, Austin, 1–12.
- [32] Yuyang Jin, Haojie Wang, Teng Yu, Xiongchao Tang, Torsten Hoefler, Xu Liu, and Jidong Zhai. 2020. ScalAna: Automating scaling loss detection with graph analysis. In SC20: International Conference for High Performance Computing, Networking, Storage and Analysis. IEEE, IEEE, Atlanta, GA, USA, 1–14.
- [33] Samuel Khuvis, Sameer Shende, Allen Malony, Neena Imam, and Manjunath Gorentla Venkata. 2018. Performance Analysis of OpenSHMEM Applications with TAU Commander. Springer, Cham, Cham, Switzerland, 161–179. doi:10.1007/978-3-319-73814-7\_11
- [34] Yudhishthira Kundu, Manroop Kaur, Tripty Wig, Kriti Kumar, Pushpanjali Kumari, Vivek Puri, and Manish Arora. 2025. A Comparison of the Cerebras Wafer-Scale Integration Technology with Nvidia GPUbased Systems for Artificial Intelligence. arXiv:2503.11698 [cs.AR] https://arxiv.org/abs/2503.11698
- [35] Hyoukjun Kwon, Prasanth Chatarasi, Vivek Sarkar, Tushar Krishna, Michael Pellauer, and Angshuman Parashar. 2020. MAESTRO: A Data-Centric Approach to Understand Reuse, Performance, and Hardware Cost of DNN Mappings. *IEEE Micro* 40, 3 (2020), 20–29. doi:10.1109/ MM.2020.2985963
- [36] Weihe Li and Paul Patras. 2024. Stable-Sketch: A Versatile Sketch for Accurate, Fast, Web-Scale Data Stream Processing. In Proceedings of the ACM Web Conference 2024 (Singapore, Singapore) (WWW '24). Association for Computing Machinery, New York, NY, USA, 4227–4238. doi:10.1145/3589334.3645581
- [37] Zeyan Li, Junjie Chen, Rui Jiao, Nengwen Zhao, Zhijun Wang, Shuwei Zhang, Yanjun Wu, Long Jiang, Leiqin Yan, Zikai Wang, Zhekang Chen, Wenchi Zhang, Xiaohui Nie, Kaixin Sui, and Dan Pei. 2021. Practical Root Cause Localization for Microservice Systems via Trace Analysis. In 2021 IEEE/ACM 29th International Symposium on Quality of Service (IWQOS). IEEE, Tokyo, Japan, 1–10. doi:10.1109/IWQOS52092.2021. 9521340
- [38] Jinjin Lin, Pengfei Chen, and Zibin Zheng. 2018. Microscope: Pinpoint Performance Issues with Causal Graphs in Micro-service Environments. In Service-Oriented Computing: 16th International Conference, ICSOC 2018, Hangzhou, China, November 12-15, 2018, Proceedings (Hangzhou, China). Springer-Verlag, Berlin, Heidelberg, 3-20. doi:10.1007/978-3-030-03596-9 1
- [39] Jinkun Lin, Ziheng Jiang, Zuquan Song, Sida Zhao, Menghan Yu, Zhanghan Wang, Chenyuan Wang, Zuocheng Shi, Xiang Shi, Wei Jia, et al. 2025. Understanding Stragglers in Large Model Training Using What-if Analysis. arXiv preprint arXiv:2505.05713 (2025), 19 pages.
- [40] Shu-Yen Lin and Jin-Yi Lin. 2017. Thermal-and performance-aware address mapping for the multi-channel three-dimensional DRAM systems. *IEEE Access* 5 (2017), 5566–5577.
- [41] Hatem Ltaief, Yuxi Hong, Leighton Wilson, Mathias Jacquelin, Matteo Ravasi, and David Elliot Keyes. 2023. Scaling the "Memory Wall" for Multi-Dimensional Seismic Processing with Algebraic Compression on Cerebras CS-2 Systems. In Proceedings of the International Conference for High Performance Computing, Networking, Storage and Analysis (Denver, CO, USA) (SC '23). Association for Computing Machinery, New York, NY, USA, Article 6, 12 pages. doi:10.1145/3581784.3627042
- [42] Ruiming Lu, Erci Xu, Yiming Zhang, Fengyi Zhu, Zhaosheng Zhu, Mengtian Wang, Zongpeng Zhu, Guangtao Xue, Jiwu Shu, Minglu Li, and Jiesheng Wu. 2023. PERSEUS: a fail-slow detection framework for cloud storage systems. In Proceedings of the 21st USENIX Conference on File and Storage Technologies (Santa Clara, CA, USA) (FAST'23).

- USENIX Association, USA, Article 4, 15 pages.
- [43] Ruiming Lu, Erci Xu, Yiming Zhang, Zhaosheng Zhu, Mengtian Wang, Zongpeng Zhu, Guangtao Xue, Minglu Li, and Jiesheng Wu. 2022. {NVMe}{SSD} failures in the field: the {Fail-Stop} and the {Fail-Slow}. In 2022 USENIX Annual Technical Conference (USENIX ATC 22). USENIX Association, Carlsbad, CA, USA, 1005–1020.
- [44] Jonathan Mace, Ryan Roelke, and Rodrigo Fonseca. 2015. Pivot tracing: dynamic causal monitoring for distributed systems. In *Proceedings* of the 25th Symposium on Operating Systems Principles (Monterey, California) (SOSP '15). Association for Computing Machinery, New York, NY, USA, 378–393. doi:10.1145/2815400.2815415
- [45] Aniruddha Marathe, Yijia Zhang, Grayson Blanks, Nirmal Kumbhare, Ghaleb Abdulla, and Barry Rountree. 2017. An empirical survey of performance and energy efficiency variation on intel processors. In Proceedings of the 5th International Workshop on Energy Efficient Supercomputing. ACM, CO, Denver, USA, 1–8.
- [46] Farhad Merchant. 2025. Architectures for Scientific Computing. Springer Nature Singapore, Singapore, 401–414. doi:10.1007/978-981-97-9314-3\_16
- [47] K. G. Müller, T.Vignaux, O. Lünsdorf, and S. Scherfke. 2002. SimPy: Discrete Event Simulation for Python. Team SimPy. https://simpy.readthedocs.io/ Accessed: 2023-11-13.
- [48] Rishiyur S Nikhil et al. 2002. Executing a program on the MIT tagged-token dataflow architecture. *IEEE Transactions on computers* 39, 3 (2002), 300–318.
- [49] Biswaranjan Panda, Deepthi Srinivasan, Huan Ke, Karan Gupta, Vinayak Khot, and Haryadi S Gunawi. 2019. {IASO}: A {Fail-Slow} Detection and Mitigation Framework for Distributed Storage Services. In 2019 USENIX Annual Technical Conference (USENIX ATC 19). USENIX Association, Renton, WA, 47–62.
- [50] Shailja Pandey, Sayam Sethi, and Preeti Ranjan Panda. 2024. 3D-TemPo: Optimizing 3D DRAM performance under temperature and power constraints. IEEE Transactions on Computer-Aided Design of Integrated Circuits and Systems 43, 8 (2024), 2263 2276.
- [51] Thanumalayan Sankaranarayana Pillai, Ramnatthan Alagappan, Lanyue Lu, Vijay Chidambaram, Andrea C Arpaci-Dusseau, and Remzi H Arpaci-Dusseau. 2017. Application crash consistency and performance with CCFS. ACM Transactions on Storage (TOS) 13, 3 (2017), 1–29.
- [52] Joseph Redmon and Ali Farhadi. 2017. YOLO9000: Better, Faster, Stronger. In 2017 IEEE Conference on Computer Vision and Pattern Recognition (CVPR). IEEE, Honolulu, HI, USA, 6517–6525. doi:10.1109/ CVPR.2017.690
- [53] Bogdan F Romanescu, Sule Ozev, and Daniel J Sorin. 2006. Quantifying the impact of process variability on microprocessor behavior. In Workshop on Architectural Reliability. Citeseer, Orlando, Florida, 10 pages.
- [54] Siva Kumar Sastry Hari, Man-Lap Li, Pradeep Ramachandran, Byn Choi, and Sarita V Adve. 2009. mSWAT: Low-cost hardware fault detection and diagnosis for multicore systems. In *Proceedings of the* 42nd Annual IEEE/ACM International Symposium on Microarchitecture. IEEE, New York, NY, USA, 122–132.
- [55] Prachi Shukla, Ayse K Coskun, Vasilis F Pavlidis, and Emre Salman. 2019. An overview of thermal challenges and opportunities for monolithic 3D ICs. In *Proceedings of the 2019 Great Lakes Symposium on VLSI*. ACM, VA, Tysons Corner, USA, 439–444.
- [56] Karen Simonyan and Andrew Zisserman. 2015. Very Deep Convolutional Networks for Large-Scale Image Recognition. arXiv:1409.1556 [cs.CV] https://arxiv.org/abs/1409.1556
- [57] George M. Slota, Sivasankaran Rajamanickam, and Kamesh Madduri. 2015. High-Performance Graph Analytics on Manycore Processors. In 2015 IEEE International Parallel and Distributed Processing Symposium. IEEE, Hyderabad, India, 17–27. doi:10.1109/IPDPS.2015.54

- [58] Christian Szegedy, Wei Liu, Yangqing Jia, Pierre Sermanet, Scott Reed, Dragomir Anguelov, Dumitru Erhan, Vincent Vanhoucke, and Andrew Rabinovich. 2015. Going deeper with convolutions. In Proceedings of the IEEE conference on computer vision and pattern recognition. IEEE, Boston, MA, USA, 1–9.
- [59] Ebadollah Taheri, Sudeep Pasricha, and Mahdi Nikdast. 2022. DeFT: A deadlock-free and fault-tolerant routing algorithm for 2.5 D chiplet networks. In 2022 Design, Automation & Test in Europe Conference & Exhibition (DATE). IEEE, IEEE, Antwerp, Belgium, 1047–1052.
- [60] Xiongchao Tang, Jidong Zhai, Xuehai Qian, Bingsheng He, Wei Xue, and Wenguang Chen. 2018. vSensor: leveraging fixed-workload snippets of programs for performance variance detection. In Proceedings of the 23rd ACM SIGPLAN symposium on principles and practice of parallel programming. ACM, Vienna Austria, 124–136.
- [61] M Bedford Taylor, Walter Lee, Saman Amarasinghe, and Anant Agarwal. 2003. Scalar operand networks: On-chip interconnect for ILP in partitioned architectures. In *The Ninth International Symposium on High-Performance Computer Architecture*, 2003. HPCA-9 2003. Proceedings. IEEE, IEEE, Anaheim, CA, USA, 341–353.
- [62] Min Tian, Junjie Wang, Zanjun Zhang, Wei Du, Jingshan Pan, and Tao Liu. 2022. swSuperLU: A highly scalable sparse direct solver on Sunway manycore architecture. J. Supercomput. 78, 9 (June 2022), 11441–11463. doi:10.1007/s11227-021-04270-w
- [63] Vasileios Tsoutsouras, Dimosthenis Masouros, Sotirios Xydis, and Dimitrios Soudris. 2017. SoftRM: Self-organized fault-tolerant resource management for failure detection and recovery in NoC based many-cores. ACM Transactions on Embedded Computing Systems (TECS) 16, 5s (2017), 1–19.
- [64] Hanzhang Wang, Zhengkai Wu, Huai Jiang, Yichao Huang, Jiamu Wang, Selcuk Kopru, and Tao Xie. 2022. Groot: an event-graph-based approach for root cause analysis in industrial settings. In Proceedings of the 36th IEEE/ACM International Conference on Automated Software Engineering (Melbourne, Australia) (ASE '21). IEEE Press, Melbourne, Australia, 419–429. doi:10.1109/ASE51524.2021.9678708
- [65] Lihuan Wang, Shuyan Jiang, Shuyu Chen, Junshi Wang, and Letian Huang. 2019. Optimized mapping algorithm to extend lifetime of both NoC and cores in many-core system. *Integration* 67 (2019), 82–94.
- [66] Pengyu Wang, Weiling Yang, Jianbin Fang, Dezun Dong, Chun Huang, Peng Zhang, Tao Tang, and Zheng Wang. 2023. Optimizing Direct Convolutions on ARM Multi-Cores. In SC23: International Conference for High Performance Computing, Networking, Storage and Analysis. ACM, CO, Denver, USA, 1–14.
- [67] Xiaodong Wang and José F. Martínez. 2015. XChange: A market-based approach to scalable dynamic multi-resource allocation in multicore architectures. In 2015 IEEE 21st International Symposium on High Performance Computer Architecture (HPCA). IEEE, Burlingame, CA, USA, 113–125. doi:10.1109/HPCA.2015.7056026
- [68] Yipeng Wang, Tong Yang, Ren Wang, and Charlie Tai. 2019. Dynamic Sketch: Efficient and Adjustable Heavy Hitter Detection for Software Packet Processing. In 2019 IEEE 8th International Conference on Cloud Networking (CloudNet). IEEE, Coimbra, Portugal, 1–7. doi:10.1109/ CloudNet47604.2019.9064148
- [69] Felix Wolf, Brian JN Wylie, Erika Abraham, Daniel Becker, Wolfgang Frings, Karl Fürlinger, Markus Geimer, Marc-André Hermanns, Bernd Mohr, Shirley Moore, et al. 2008. Usage of the SCALASCA toolset for scalable performance analysis of large-scale parallel applications. In Tools for High Performance Computing: Proceedings of the 2nd International Workshop on Parallel Tools for High Performance Computing, July 2008, HLRS, Stuttgart. Springer, Springer Berlin Heidelberg, Berlin, Heidelberg, 157–167.
- [70] Tianyuan Wu, Wei Wang, Yinghao Yu, Siran Yang, Wenchao Wu, Qinkai Duan, Guodong Yang, Jiamang Wang, Lin Qu, and Liping Zhang. 2024. FALCON: Pinpointing and Mitigating Stragglers for Large-Scale Hybrid-Parallel Training. arXiv:2410.12588 [cs.DC] https://arxiv.org/

- abs/2410.12588
- [71] Siyuan Xiao, Xiaohang Wang, Maurizio Palesi, Amit Kumar Singh, and Terrence Mak. 2019. ACDC: An accuracy-and congestion-aware dynamic traffic control method for networks-on-chip. In 2019 Design, Automation & Test in Europe Conference & Exhibition (DATE). IEEE, IEEE, Florence, Italy, 630–633.
- [72] Zheng Xu, Dehao Kong, Jiaxin Liu, Jinxi Li, Jingxiang Hou, Xu Dai, Chao Li, Shaojun Wei, Yang Hu, and Shouyi Yin. 2025. WSC-LLM: Efficient LLM Service and Architecture Co-exploration for Wafer-scale Chips. In Proceedings of the 52nd Annual International Symposium on Computer Architecture (ISCA '25). Association for Computing Machinery, New York, NY, USA, 1–17. doi:10.1145/3695053.3731101
- [73] Zikang Xu, Yiming Zhang, and Zhirong Shen. 2025. A Fail-Slow Detection Framework for HBM Devices. In Proceedings of the 30th Asia and South Pacific Design Automation Conference. USENIX Association, Santa Clara, CA, 491–497.
- [74] Lingxiang Yin, Amir Ghazizadeh, Ahmed Louri, and Hao Zheng. 2023. ARIES: Accelerating Distributed Training in Chiplet-Based Systems via Flexible Interconnects. In 2023 IEEE/ACM International Conference on Computer Aided Design (ICCAD). IEEE, San Francisco, CA, USA, 1–9. doi:10.1109/ICCAD57390.2023.10323955
- [75] Xin You, Zhibo Xuan, Hailong Yang, Zhongzhi Luan, Yi Liu, and Depei Qian. 2024. GVARP: Detecting Performance Variance on Large-Scale Heterogeneous Systems. In SC24: International Conference for High Performance Computing, Networking, Storage and Analysis. IEEE, IEEE, Atlanta, GA, USA, 1–16.
- [76] Guangba Yu, Pengfei Chen, Hongyang Chen, Zijie Guan, Zicheng Huang, Linxiao Jing, Tianjun Weng, Xinmeng Sun, and Xiaoyun Li. 2021. MicroRank: End-to-End Latency Issue Localization with Extended Spectrum Analysis in Microservice Environments. In Proceedings of the Web Conference 2021 (Ljubljana, Slovenia) (WWW '21). Association for Computing Machinery, New York, NY, USA, 3087–3098. doi:10.1145/3442381.3449905
- [77] Jidong Zhai, Wenguang Chen, and Weimin Zheng. 2010. PHANTOM: predicting performance of parallel applications on large-scale parallel machines using a single node. In *Proceedings of the 15th ACM SIGPLAN Symposium on Principles and Practice of Parallel Programming* (Bangalore, India) (*PPoPP '10*). Association for Computing Machinery, New York, NY, USA, 305–314. doi:10.1145/1693453.1693493
- [78] Lei Zhang, Zhiqiang Xie, Vaastav Anand, Ymir Vigfusson, and Jonathan Mace. 2023. The Benefit of Hindsight: Tracing Edge-Cases in Distributed Systems. In 20th USENIX Symposium on Networked Systems Design and Implementation (NSDI 23). USENIX Association, Boston, MA, 321–339. https://www.usenix.org/conference/nsdi23/presentation/ zhang-lei
- [79] Nathan Zhang, Rubens Lacouture, Gina Sohn, Paul Mure, Qizheng Zhang, Fredrik Kjolstad, and Kunle Olukotun. 2024. The Dataflow Abstract Machine Simulator Framework. In Proceedings of the 51st Annual International Symposium on Computer Architecture (ISCA '24). IEEE Press, Buenos Aires, Argentina, 532–547. doi:10.1109/ISCA59077. 2024.00046
- [80] Hao Zheng, Ke Wang, and Ahmed Louri. 2021. Adapt-noc: A flexible network-on-chip design for heterogeneous manycore architectures. In 2021 IEEE international symposium on high-performance computer architecture (HPCA). IEEE, IEEE, Seoul, Korea (South), 723–735.
- [81] Lianmin Zheng, Zhuohan Li, Hao Zhang, Yonghao Zhuang, Zhifeng Chen, Yanping Huang, Yida Wang, Yuanzhong Xu, Danyang Zhuo, Eric P. Xing, Joseph E. Gonzalez, and Ion Stoica. 2022. Alpa: Automating Inter- and Intra-Operator Parallelism for Distributed Deep Learning. In 16th USENIX Symposium on Operating Systems Design and Implementation (OSDI 22). USENIX Association, Carlsbad, CA, 559– 578. https://www.usenix.org/conference/osdi22/presentation/zhenglianmin

- [82] Liyan Zheng, Jidong Zhai, Xiongchao Tang, Haojie Wang, Teng Yu, Yuyang Jin, Shuaiwen Leon Song, and Wenguang Chen. 2022. Vapro: Performance variance detection and diagnosis for production-run parallel applications. In Proceedings of the 27th ACM SIGPLAN Symposium on Principles and Practice of Parallel Programming. ACM, Seoul, Republic of Korea, 150–162.
- [83] Minxuan Zhou, Andreas Prodromou, Rui Wang, Hailong Yang, Depei Qian, and Dean Tullsen. 2019. Temperature-aware dram cache management—relaxing thermal constraints in 3-d systems. IEEE Transactions on Computer-Aided Design of Integrated Circuits and Systems 39, 10 (2019), 1973–1986.